Exploring the effects of seismicity on landslides and catchment sediment yield: An Italian case study

Article *in* Geomorphology · November 2016

DOI: 10.1016/j.geomorph.2016.11.010

CITATIONS
0

READS
106

4 authors:

Matthias Vanmaercke
University of Leuven
51 PUBLICATIONS **781** CITATIONS
SEE PROFILE

Francesca Ardizzone
Italian National Research Council
82 PUBLICATIONS **2,332** CITATIONS
SEE PROFILE

Mauro Rossi
Italian National Research Council
135 PUBLICATIONS **2,488** CITATIONS
SEE PROFILE

Fausto Guzzetti
Italian National Research Council
365 PUBLICATIONS **10,625** CITATIONS
SEE PROFILE

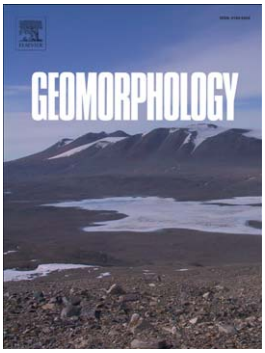

Exploring the effects of seismicity on landslides and catchment sediment yield: An Italian case study

Matthias Vanmaercke, Francesca Ardizzone, Mauro Rossi, Fausto Guzzetti

PII: S0169-555X(16)31069-8
DOI: doi: 10.1016/j.geomorph.2016.11.010
Reference: GEOMOR 5832

To appear in: *Geomorphology*

Received date: 23 December 2015
Revised date: 25 October 2016
Accepted date: 12 November 2016

Please cite this article as: Vanmaercke, Matthias, Ardizzone, Francesca, Rossi, Mauro, Guzzetti, Fausto, Exploring the effects of seismicity on landslides and catchment sediment yield: An Italian case study, *Geomorphology* (2016), doi: 10.1016/j.geomorph.2016.11.010

Exploring the effects of seismicity on landslides and catchment sediment yield: an Italian case study

Matthias Vanmaercke [a,b,*], Francesca Ardizzone [c], Mauro Rossi [c], Fausto Guzzetti [c]

[a] KU Leuven, Department of Earth and Environmental Sciences, Leuven, Belgium

[b] Research Foundation Flanders (FWO), Brussels, Belgium

[c] Consiglio Nazionale delle Ricerche, Instituto di Ricerca per la Protezione Idrogeologica, via della Madonna Alta 126, 06128 Perugia, Italy

[*] Corresponding author at: Department of Earth and Environmental Sciences, KU Leuven, Belgium. Tel: +32 16376127. E-mail address: matthias.vanmaercke@kuleuven.be

Abstract

Recent studies showed that contemporary average catchment sediment yields (*SY*, t km^{-2} y^{-1}]) at regional and continental scales are often strongly correlated to spatial patterns of seismic activity. Nonetheless, we currently have little insights into the mechanisms that explain these correlations. We investigated how spatial patterns of *SY* in Italy are linked to patterns of seismic activity. For a dataset of 103 Italian catchments with average *SY* measured over a period of years to decades, we extracted tectonic and none-tectonic variables that potentially explain observed differences in *SY*. These include proxies for vertical uplift rates and cumulative seismic moments (*CSM*) associated with historic earthquakes of different ranges of magnitude. Results showed that also across Italy, *SY* is significantly correlated to seismicity. However, *SY* showed much stronger correlations with proxies of seismicity relating to small but frequent earthquakes ($2 \leq M_w < 4$) than with proxies relating to tectonic uplift or large, potentially landslide-triggering earthquakes ($M_w \geq 4$). Analyses of a dataset of about 500,000 landslides across Italy showed very comparable trends: spatial patterns of landslides within similar lithological units generally show a significant positive correlation with *CSM* of weak but frequent seismicity and generally not with *CSM* of large earthquakes. These results suggest that, on a decadal time scale and at a regional/continental spatial scale, frequent but relatively weak seismicity may exert a more important geomorphic impact than large earthquake events or tectonic uplift.

Keywords: Earthquake, Uplift, Peak ground acceleration, Landslide, Sediment yield, Italy.

1. Introduction

Understanding geomorphic processes and contemporary sediment yield (*SY*, t km^{-2} y^{-1}) at regional and continental scales is highly relevant for a wide range of ecological, economic and scientific reasons (Meybeck, 2003; Owens et al., 2005; Syvitski and Milliman, 2007; Vanmaercke et al., 2011a; de Vente et al., 2013). Spatial differences in *SY* and contemporary erosion processes have been linked to differences in topography, lithology, climate, and land use (e.g., Owens et al., 2005; Syvitski and Milliman, 2007). However, there is growing evidence that, both on contemporary and millennial time scales, seismicity can exert a dominant influence on regional patterns of catchment *SY* (Dadson et al., 2003; Portanga and Bierman, 2011; Vanmaercke et al., 2014a,b,c).

The processes explaining these strong correlations between seismicity and *SY* at regional scales are currently poorly understood. As discussed by Vanmaercke et al. (2014a), several potential mechanisms are possible. First, seismicity can be strongly correlated to tectonic uplift. In such cases, observed correlations between seismicity and *SY* may be attributable to river incision, topographic steepening, and increased mass wasting in response to this uplift. Several studies have provided evidence for such mechanism (e.g., Montgomery and Brandon, 2002; DiBiasi et al., 2010; Larsen and Montgomery, 2012). Nonetheless, these studies mainly focus on strongly uplifting areas, and on sediment fluxes over time periods of thousands to millions of years. Very few studies have explored the link between contemporary uplift rates and contemporary *SY* (at timescales of years to decades). Moreover, the correlations between seismicity and *SY* also hold for regions that are currently not uplifting (e.g., Vanmaercke et al., 2014a,b). Therefore, tectonic uplift alone cannot explain observed correlations between seismicity and *SY*.

Second, large earthquakes can trigger numerous landslides that significantly affect *SY* over the course of several years (e.g. Pearce and Watson, 1986; Dadson et al., 2003; Malamud et al., 2004; Koi et al., 2008; Hovius et al., 2011; Marc et al., 2015). While earthquake-triggered landsliding is certainly a highly relevant process in several tectonically highly active regions, it cannot explain all observed correlations between seismicity and *SY* at regional scales. For example, overall only large earthquakes (typically $M_w \geq 4$) can directly trigger landslides (Keefer, 1984; Malamud et al., 2004; Sidle and Ochiai, 2006; Keefer, 2013). However, correlations between seismicity and *SY* have also been observed across regions where such large earthquakes occur only rarely or not at all (e.g., Vanmaercke et al., 2014a,b).

Third, seismicity may influence *SY* by weakening lithology (e.g., by fracturing) and so enhancing the rate at which various erosion processes may take place (e.g., Molnar et al., 2007; Koons et al., 2012). One of these processes is landsliding. Various studies indicate that seismicity or rock fracturing can strongly increase the likelihood of having landslides, without directly triggering them (e.g., Huang et al., 2013; Marc et al., 2015; Carlini et al., 2016; Bucci et al., 2016). The occurrence of small but frequent seismic events may play an important role in this. Some studies indicate that also other erosion processes, such as gully erosion, may be strongly influenced by the occurrence of weak but frequent earthquakes (e.g., Cox et al., 2010).

These are all plausible mechanisms that each may contribute to observed correlations between seismicity and *SY*. However, their relative importance in different tectonic and geomorphic environments remains poorly understood. Our understanding could benefit from studies that disentangle the impact of uplift, large (but infrequent) earthquakes, and weak (but frequent) seismicity on *SY* and geomorphic processes at regional and continental scales. This work aims to explore the relative importance of the different mechanisms in explaining spatial patterns of *SY* and landslides across Italy. Italy was chosen as a study area as it offers a large range of tectonic and seismic conditions, and has detailed measurements on *SY* (e.g., Vanmaercke et al., 2011b), seismicity (Selvaggi et al., 1997; Rovida et al., 2011; ISIDE, 2015), landslides (APAT, 2007), and contemporary uplift or subduction rates (Serpelloni et al., 2013).

2. Materials and methods

2.1. Quantifying seismicity

Many studies focusing on the link between seismicity and *SY* have used seismic hazard maps to quantify the degree of seismic activity (e.g., Portenga and Bierman, 2011; Vanmaercke et al., 2014a,b,c). Such maps indicate the maximum peak ground acceleration (*PGA*) that is expected to occur due to earthquakes with a predefined recurrence interval (typically 475 years; e.g., SHARE, 2013). As discussed in these studies, expected *PGA* provides a meaningful proxy for seismicity that works very well as a predictor of *SY*. A major advantage is that *PGA* provides an estimate of the expected seismicity for every point in space. However, this proxy also has some important shortcomings. First, expected *PGA* values are subject to important uncertainties as they require estimating the probability of high-magnitude earthquakes. Second, *PGA* is a time-unspecific measure that is not necessarily related to the seismicity that occurred during the *SY* measuring period. Third, the *PGA* values mainly relate

to the expected largest earthquake in a region, and provide no direct information on weaker but more frequent earthquakes. As a result of the Gutenberg-Richter law, strong correlations between PGA and the overall rate of seismicity can be expected (e.g., Turcotte and Malamud, 2004). Nevertheless, expected *PGA* does not allow differentiating between earthquakes of different magnitudes and frequencies.

Other studies (e.g., Selvaggi et al., 1997; Dadson et al., 2003) quantified seismicity by means of cumulative seismic moments (*CSM*). *CSM* overcomes many of the problems outlined above, as it can be calculated for sets of earthquakes within a specific time interval and magnitude range. However, seismic moments are typically associated with one point in space (i.e., the epicenter; Selvaggi et al., 1997) while earthquakes typically affect larger areas. The geomorphic impacts of an earthquake on any given location (e.g., the probability of triggering a landslide) depend not only on the moment magnitude but, among other factors, also on the distance from the epicenter (e.g., Keefer, 2002; Meunier et al., 2007). Hence, the seismic moment (i.e., the energy release) associated with an earthquake should be realistically distributed over a wider area. We therefore constructed *CSM* maps where the energy associated with each earthquake was distributed over a wider area, proportionally to the estimated spatial pattern of peak ground acceleration associated with the earthquake.

From the Italian Seismological Instrumental and Parametric Database (ISIDE, 2015), we selected all earthquakes that have occurred in Italy, or less than 50 km from its borders, between 1 January 1985 (i.e., the start date of the systematic recording) and 31 December 2014, with a reported magnitude (e.g., M_L, M_B and M_w) $\geq$ 2. This was done because earthquakes with smaller magnitudes were insufficiently represented in the database. To this selection, we added all earthquakes of $M_w \geq 5$ that occurred between 1900 and 1985, as registered in the CPTI-catalogue of paleo-seismic events (Rovida et al., 2011). This creates a slight inconsistency in the time periods over which earthquakes are considered: earthquakes with an $M_w < 5$ are considered only for the period 1985–2014, while earthquakes with an $M_w \geq 5$ are considered for the period 1900–2014. We maintain that this is justified, given the fact that we are mainly interested in studying how regional patterns of earthquakes with specific magnitudes relate to spatial patterns of *SY* and landslides. Given the fact that only few earthquakes with $M_w \geq 5$ occurred during the 30-year period 1985–2014, considering only the large earthquakes since 1985 would result in too few events to generate a statistical meaningful pattern. In total, this resulted in a dataset of 72,127 earthquakes.

For each selected earthquake, we calculated its seismic moment (*M*o, N.m) by either directly converting the reported moment magnitude or, when no moment magnitude was given, by converting the reported magnitude using previously proposed empirical relationships (Selvaggi et al., 1997; Scordilis, 2006). Next, we generated a raster map with a spatial resolution of 1×1 km indicating *PGA* associated with that earthquake. *PGA* values of each cell were estimated using the empirical equation proposed by Bindi et al. (2009),

$$\log_{10}(PGA) = \mathrm{a} + \mathrm{b}M + \mathrm{c}\log_{10}\sqrt{R^2 + \mathrm{h}^2} + l \qquad (1)$$

where *PGA* is the maximum peak ground acceleration associated with the considered earthquake [cm s^{-2}]; M the earthquake magnitude; R the epicentral distance [km]; a, b, c, and h empirical coefficients (a = 1.344, b = 0.328, c = -1.09, h = 5); and *l* a term that allows to adapt the PGA estimate based on the lithological conditions of the site (0 for rock, 0.262 for shallow alluvium and 0.096 for deep alluvium; Bindi et al., 2009). Due to the lack of accurate data on the depth of alluvium, and the fact that this term may induce spurious correlation with lithology, all PGA values were simulated under the assumption of a 'rock' lithology (*l* = 0). Eq. (1) was originally calibrated using 235 carefully selected ground motion measurements recorded at 137 stations across Italy, for 27 earthquakes with $4.60 \leq M_w < 6.96$ (Bindi et al., 2009).

The obtained raster was then used as a proxy to distribute *M*o of the earthquake over the area around the epicenter. More specifically, the seismic moment was distributed over the study area as follows:

$$SM_{EQ,i} = \frac{PGA_i \times SM_{EQ}}{\sum_{i=1}^{n} PGA_i} \qquad (Eq.\ 2)$$

$SM_{EQ,i}$ is the estimated seismic moment in cell *i* associated with the earthquake *EQ*, PGA_i is the estimated peak ground acceleration in cell *i* associated with *EQ* (based on Eq. 1), and *n* is the total number of cells in the study area. Using Eqs. (1) and (2), we generated a seismic moment distribution map for each of the 72,127 selected earthquakes. The resulting maps were then added up to produce maps of *CSM*. Separate *CSM* maps were generated for all earthquakes with $2 \leq M_w < 3$ ($CSM_{2\text{-}3}$), $3 \leq M_w < 4$ ($CSM_{3\text{-}4}$), $4 \leq M_w < 5$ ($CSM_{4\text{-}5}$), $5 \leq M_w < 6$ ($CSM_{5\text{-}6}$) and $6 \leq M_w$ (CSM_{6+}). The maps were normalized for the length of the observation record. More specifically, values of the $CSM_{5\text{-}6}$ and CSM_{6+} maps were divided by 115 years (1900–2014). Values of the other maps were divided by 30 years (1985–2014). Adding up these magnitude-specific *CSM* maps allowed generating *CSM* maps for all selected earthquakes with $M_w \geq 2$ (CSM_{All}), all earthquakes with $2 \leq M_w < 4$ ($CSM_{2\text{-}4}$) and all

earthquakes with $M_w \geq 4$ (CSM_{4-8}). The distinction between CSM_{2-4} and CSM_{4-8} was made since it is expected that only earthquakes of $M_w \geq 4$ can directly trigger landslides (e.g., Keefer, 2002; 2013; Malamud et al., 2004).

Our approach relies on some assumptions. First, our method assumes that *PGA* provides a realistic proxy for the actual energy dissipation of the earthquake. Such assumption is justified by the close physical relation between force and acceleration, as well as by empirical evidence. For example, Eq. (1) implies that that *PGA* decreases exponentially with the distance from the epicenter. This concurs with numerous studies showing that in the case of landslide-triggering earthquake events, the landslide density also decreases exponentially with the distance from the epicenter (Keefer, 2002, 2013), whereas the density of landslides triggered by a specific earthquake is generally linearly related to *PGA* (Meunier et al., 2007). Second, our approach does not consider all factors that may influence *PGA*, such as lithology, hypocenter depth, faulting mechanism, and local topography (Meunier et al., 2008; Bindi et al., 2009). Nevertheless, earthquake magnitude and distance from the epicenter can be expected to be the most important proxies to estimate *PGA* on a given location (Bindi et al., 2009). Hence, we are confident that our approach allows characterizing general patterns of seismicity at regional and decadal time scales.

2.2. Catchment sediment yield data and selection of the catchments

Based on an extensive literature review, Vanmaercke et al. (2011b) compiled a database of average *SY* observations in Europe that were derived either from reservoir sedimentation rates, or from runoff discharge and sediment concentration measurements at gauging stations over a measuring period of at least one year. For each of the Italian catchments included in this database, we delineated the contributing area using standard GIS procedures and available digital elevation models (DEMs) (Lehner et al., 2006; CGIAR, 2008). However, for several catchments, there were large discrepancies between the size of the delineated area and the catchment area reported in the original source of the data. Such discrepancies are not uncommon, and can be attributed to several potential causes including inaccuracies in the reported catchment outlet, errors in the DEM flow accumulation, and errors in the originally reported catchment areas (see Vanmaercke et al., 2014b for a discussion). Nonetheless, such deviations can cause important uncertainties when analyzing correlations between *SY* and catchment characteristics. Therefore, we considered only those catchments for which the size of the delineated area deviated less than 20% from the originally reported catchment area.

In total, 103 catchments with *SY* observations were retained for this study (**Fig. 1**). *SY* values ranged between 0.9 and 4568 t $km^{-2}y^{-1}$. As mentioned above, these *SY* observations were compiled from a number of sources (Gazzolo and Bassi, 1960; Tropeano, 1984; Tamburino, 1990; Ufficio Idrografico e Mareografico, 1997, Ferro et al., 2003; Meybeck and Ragu, 1995; Lenzi et al., 2003; Van Rompaey et al., 2005; Torri et al., 2006; Pavanelli and Rigotti, 2007) and were based on different measuring methods over different measuring periods. For 59 of the 103 catchments, the *SY* value was derived from gauging station observations, whereas for the other 44 catchments the *SY* was derived from reservoir sedimentation rates. Measuring periods varied in length between 1 and 60 years (median: ca. 20 years). Measuring periods varied between 1908 and 2003, with most of the *SY* measurements conducted around 1950–1960. For some of the *SY* observations, the exact measuring period was unclear (e.g., because only the length of the measuring period was reported; Vanmaercke et al., 2011b).

The fact that our *SY* data were derived from a variety of studies using different techniques complicates our analyses to some extent. For example, most *SY* values based on gauging station observations consider only suspended load, whereas *SY* data derived from reservoir sedimentation rates comprise both suspended load and bed load. It is also well known that the accuracy of average *SY* values depends strongly on the measuring procedure used (Phillips et al., 1999; Verstraeten and Poesen, 2002; Moatar et al., 2006) and the duration of the measuring period (Vanmaercke et al., 2012). Hence, also the reliability of the *SY* values may strongly vary. In most cases, insufficient details were reported to accurately quantify the uncertainties. Such difficulties are not unique to this study, but affect most studies aiming to study *SY* at regional or continental scales (de Vente et al., 2006; Syvitski and Milliman, 2007; de Vente et al., 2011; Vanmaercke et al., 2014a,b). However, as these studies show, the uncertainties do not prevent the detection of meaningful relations between *SY* and geomorphic/tectonic factors. They limit only the extent to which variability in *SY* can be explained (Vanmaercke et al., 2014a,b). Moreover, most of the *SY* data considered in this study can be expected to be fairly reliable and certainly belong to the more accurate *SY* data available for Europe (Vanmaercke et al., 2011b). The *SY* observations from gauging stations are generally based on high frequency sampling (> 1 sample/week), while *SY* observations from sedimentation rates were corrected for the reservoir trapping efficiency (which was generally very high). In addition, the measuring period of most *SY* observations was fairly long (mostly ≥ 10 years) Previous studies showed that especially these factors strongly

influence the reliability of average *SY* values (Phillips et al., 1999; Verstraeten and Poesen, 2002; Moatar et al., 2006).

2.3. Catchment characteristics and statistical analyses

For each of the 103 selected catchments (**Fig. 1**), catchment characteristics relating to the drainage area, topography, lithology, soil properties, climate, land use, reservoir impacts, and seismic/tectonic activity of the catchment were determined to explain potentially the observed differences in *SY*. An overview of all considered characteristics and their data sources is given in **Table 1**. Many of these characteristics were used in other studies aiming to explain patterns of *SY* at regional or continental scales, and are not discussed in detail here (e.g., Aalto et al., 2006; Syvitski and Milliman, 2007; de Vente et al., 2011, 2013; Vanmaercke et al. 2014a,b,c). Many more variables other than the ones used in this work and listed in **Table 1** could be considered. However, since our research mainly aims at better understanding the link between seismicity and *SY*, and not at comprehending the role of all possible factors controlling *SY*, we limited the number variables relating to none-tectonic factors.

The role of lithology and soil properties was considered somewhat differently in this study as compared with other regional or continental *SY* studies. Many studies account for lithology by assigning a score to different lithological units, where higher scores indicate an overall higher susceptibility to erosion processes (e.g., Aalto et al., 2006; de Vente et al., 2006; Syvitski and Milliman, 2007; Vanmaercke et al., 2014a,b). Such scores are often somewhat arbitrary, and do not account for the fact that susceptibility may vary depending on the erosion process considered. Here, we extracted the average soil erodibility factor (K_{st}) for each catchment, based on a recently published dataset (Panagos et al., 2014) to account for the susceptibility of soils to water erosion processes (i.e., sheet, rill, and gully erosion). However, the K_{st} values provide no information on the susceptibility of each lithology to landsliding. For this reason, we included in our analyses a lithology factor (L) that provides a first-order proxy for the lithological weakness in terms of landsliding. Using a previously published reclassified lithological map of Italy (Cardinali et al., 2013), we calculated the proportion of the area of each major lithological unit in Italy that was mapped as a landslide according to the national IFFI landslide inventory (Rovida et al., 2011), and we normalized this proportion for the average slope of the lithological unit i.e., we divided the landslide fraction by the average slope of the lithological unit and multiplied the result by the average terrain slope value for Italy (**Table 2**). The L value of each catchment was then calculated as the area-weighted average of the normalized landslide fractions of the lithological types in the catchment.

Given the scope of our study, we included a large number of variables relating to the degree of seismicity and tectonic activity in each catchment (**Table 1**, **Fig. 2**). These variables include spatially averaged *CSM* values based on different ranges of earthquake magnitudes, which were directly extracted from the constructed *CSM* maps (see **Section 2.1**). To compare the performance of the *CSM* maps with previously used proxies for seismicity, we calculated average maximum expected PGA values for different recurrence intervals (i.e., 73, 102, 475, 975, 2475, and 4975 years). These values were derived from previously constructed seismic hazard maps (SHARE, 2013). Proxies for contemporary vertical tectonic movements were derived from a study by Serpelloni et al. (2013) who constructed a map of estimated contemporary vertical ground velocities throughout Italy using measurements from a large number of geodetic stations. We used this dataset to obtain a proxy of the current vertical uplift or subsidence rates in each catchment. For each catchment, we extracted the mean, maximum, and minimum vertical velocities (VD_{avg}, VD_{max}, and VD_{min}) as well as the range in vertical velocity ($VD_{max} - VD_{min}$) divided by the catchment area (VD_{range}) i.e., a crude proxy for the overall deformation rate of the catchment.

Similar to other regional and continental *SY* studies (e.g., Aalto et al., 2006; Syvitski and Milliman, 2007; de Vente et al., 2011; Vanmaercke et al., 2014a,b,c), we explored the statistical significance of the potential controlling factors in explaining *SY* by means of regression analyses, correlation analyses, and partial correlation analyses. Partial correlation measures the degree of association between two variables, with the effect of other controlling variables removed (Fisher, 1924; Steel and Torrie, 1960). This is done by conducting a regression between each of the considered variables and the control variables and by then calculating the correlation between the residues of these two regressions. We used non-parametric Spearman rank correlation coefficients for our (partial) correlation analyses, as these do not depend on the distribution of the data (Steel and Torrie, 1960). Given the fact that our *SY* data and several of the considered variables vary over several orders of magnitude (**Table 1**), the non-parametric rank correlation coefficients can be expected to give more robust results.

2.4. Exploring the importance of seismicity for landsliding

As explained in Section 1, landslides may play an important role in explaining the link between seismicity and *SY*. Therefore, we explored the extent to which measures of seismicity (i.e., $CSM_{2\text{-}4}$ and $CSM_{4\text{-}8}$) may explain spatial patterns of known landslides. We did this by

comparing the distribution of *CSM* values of the (1×1 km) grid cells in which a landslide occurred according to the national IFFI landslide inventory (Rovida et al., 2011), with the distribution of *CSM* values of grid cells free of known landslides. Given the fact that lithology may strongly influence the probability on landslides, the analyses were conducted separately for each major lithological unit (**Table 2**). When the distribution of *CSM* values is significantly higher for pixels with landslides than those without landslides (according to a Wilcoxon rank-sum test), this provides a clear indication that seismicity positively influences the patterns of landslides within that lithological unit.

As a complementary approach, we calculated the degree of correlation between the *CSM* value and the corresponding mapped landslide fraction (*LF*) for all (1×1 km) grid cells in each lithological unit (**Table 2**). The correlations were calculated based on the Spearman rank correlation coefficient (Steel and Torrie, 1960). Additionally, we calculated the corresponding partial Spearman rank coefficients after controlling for the average slope of each grid cell. This allows us to account for the fact that, within a given lithological unit, topography, seismicity and landslide occurrence may be inter-correlated.

3. Results

3.1. Controlling factors of catchment sediment yield

Table 3 lists the Spearman rank correlation coefficients between the considered potential controlling factors (**Table 1**) and *SY*. **Fig. 3** shows scatterplots of *SY* versus some of the considered non-tectonic factors. Most correlations are relatively weak, and in some cases counter-intuitive. For example, average catchment slope shows a weak but significant negative correlation with *SY* (**Table 3**, **Fig. 3a**). Average catchment slope is also negatively correlated to many of the considered seismic variables, and to *L*. The latter, which relates to the lithological susceptibility to landsliding (**Table 2**), shows a highly significant correlation with *SY* (**Table 3**, **Fig. 3b**). K_{st} i.e., the factor relating to the soil erodibility in terms of water erosion processes (**Table 1**), does not exhibit a significant correlation with *SY*. Variables related to the land use (i.e., AL and FOREST, **Table 1**) also do not shows significant correlations with *SY* (**Table 3**, **Fig. 3c**). Of the considered climatic factors, only the average air temperature (*T*) shows a positive correlation with *SY*, whereas factors related to rainfall (intensity) or runoff show weak, but negative correlations (**Table 1**, **Fig. 3d**). We found no evidence that our correlation results are affected significantly by the presence of reservoirs in the upstream part of the catchment, or by the method used to measure *SY* (**Tables 1** and **3**).

Fig. 4 shows scatterplots of *SY* versus some of the considered catchment characteristics relating to tectonic activity (**Table 1**). The average vertical velocity of each catchment (VD_{avg}, i.e., a proxy for the contemporary uplift or subduction rate) shows a significantly negative correlation to *SY* (**Fig. 4a**), but is also negatively correlated to L and most of the proxies relating to seismicity (**Table 3**). Partial correlation analyses showed that after controlling for this inter-correlation with *L* or seismicity, the negative correlation between VD_{avg} and *SY* becomes insignificant. VD_{range} (**Table 1**) shows an insignificant correlation with *SY* (**Table 3**).

All variables related to seismicity show significant to highly significant positive correlations with *SY* (**Table -3**, **Fig. 4b-d**). For the cumulative seismic moments based on all considered earthquakes (CSM_{All}; **Table 1**) this correlation is fairly weak (**Fig. 4b**). Given the fact that the *CSM* values associated with large earthquakes are much larger than those associated with small earthquakes (see e.g., ranges in **Table 1**), CSM_{All} is almost perfectly correlated with the *CSM* values associated with large earthquakes ($M_w \geq 4$; **Table 3**). However, *CSM* values based on smaller earthquakes show a consistently stronger correlation with *SY* than those based on larger magnitudes (**Fig. 5**; **Table 3**). While the correlation between *SY* and *CSM* based on large earthquakes is fairly low, *CSM* values based on small but frequent earthquakes (M_w 2 to 4) show a highly significant correlation with *SY* (**Fig. 4c**). Also variables relating to expected PGA showed significant correlations with *SY* (**Table 3**, **Fig. 4d**). The degree of correlation tends to decrease with increasing recurrence interval (i.e., with increasing expected earthquake magnitude, but within a relatively limited range (**Table 3**, **Figs. 4** and **5**).

As can be seen in **Table 3**, many of the proxies related to seismicity are also strongly correlated to *L*. Hence, significant correlations between *CSM* and *SY* may be attributable to lithology, or vice versa. Partial correlation analyses showed that the correlations between *SY* and $CSM_{4\text{-}5}$, $CSM_{5\text{-}6}$, CSM_{6+} and all considered *PGA* values become insignificant ($p > 0.05$) after controlling for *L*. However, the partial correlation between *SY* and $CSM_{2\text{-}3}$, $CSM_{3\text{-}4}$, $CSM_{2\text{-}4}$, $CSM_{4\text{-}8}$ and CSM_{All} remained significant. On the other hand, the partial correlation between *SY* and *L* remained significant after controlling for any of the considered seismic proxies. This indicates that each of lithology and several of the proxies of seismicity (mainly those relating to weak but frequent seismicity) explain a significant part of the observed regional variation in *SY* that cannot be attributed to inter-correlations. Also *T* shows a positive correlation with both *SY* and most of our proxies relating to seismicity (**Table 3**). *SY* showed an insignificant ($p > 0.05$) partial correlation with CSM_{All}, $CSM_{4\text{-}8}$ and CSM_{6+} after controlling

for *T*. However, all other seismic variables remained significantly correlated to *SY* after removing the effect of *T*.

3.2. Links between seismicity and landslides

Fig. 6 compares the distribution in *CSM* of 1×1 km grid cells with and without landslides in the IFFI inventory (APAT, 2007), for the considered lithological types (**Table 2**). The graph shows that for most lithological types (10 out of the 14), the median $CSM_{2\text{-}4}$ is significantly higher in grid cells with landslides than in grid cells without landslides ($p < 0.05$, Wilcoxon rank-sum test). *CSM* values based on earthquakes with $M_w \geq 4$ revealed a different pattern. For 6 of the 14 considered lithological types, the median $CSM_{4\text{-}8}$ value was significantly higher in grid cells with landslides than in grid cells without landslides (**Fig. 6**).

Fig. 7 shows the non-parametric Spearman rank correlation coefficient between the fraction of landslides in each grid cell (*LF*, ranging between 0 and 1) and its corresponding *CSM* value. For most lithologies, there is a significant positive correlation between *LF* and $CSM_{2\text{-}4}$. However, correlations between *LF* and $CSM_{4\text{-}8}$ are weaker, not significant, or even negative. **Fig. 7** also shows the partial Spearman correlation coefficients between *LF* and $CSM_{2\text{-}4}$ or $CSM_{4\text{-}8}$ after controlling for the average slope of each grid cell. These correlations reveal a close agreement with the full Spearman correlation coefficients, indicating that the observed correlations between seismicity and *LF* in a lithological group are not attributable to inter-correlations with topography.

With nearly 500,000 landslides, the IFFI inventory is the most extensive landslide inventory currently available for Italy (APAT, 2007). Nonetheless, the inventory remains incomplete, and in some areas the number of landslides is underestimated (Trigila et al., 2010; Marchesini et al., 2014). We therefore investigated to what extent our results on the link between seismicity and landsliding could be affected by mapping biases in this dataset. This was done by excluding those regions for which the IFFI inventory was expected to be unreliable or incomplete (Trigila et al., 2010) and redoing our analyses for a subset of Italian regions in which the inventory was expected to be reliable. Very similar results were obtained for the lithological types that were still represented in this subset, indicating that the results of our analyses are not attributable to mapping biases.

4. Discussion

4.1. Overall interpretation of the results of the correlation analysis

At first glance, many of the correlations between *SY* and non-tectonic potential controlling factors appear to be relatively weak or even counter-intuitive (**Table 3**, **Fig. 3**). For example, land use showed no strong correlations with *SY* while topography unexpectedly showed a negative correlation with *SY*. Also climatic variables showed only weak or insignificant correlations with *SY*. To some extent, these weak correlations are attributable to uncertainties in the *SY* data. As discussed in **Section 2.1**, these were derived from a range of sources applying different techniques. While most *SY* data are expected to be fairly reliable, uncertainties are inevitable and will induce scatter on the observed correlations. Also the considered potential controlling factors (**Table 1**) induce uncertainties. For example, the considered climatic variables indicate only estimated average values of a certain period, while the variables relating to land use provide only an indication of the land cover conditions at a specific moment (i.e., 1990). These do not necessarily correspond to the potentially dynamic weather and land cover conditions during the *SY* measuring period, nor do they account for the fact that Italy (as many other Mediterranean regions) has known a very long, complex and often intense history of human impacts that may still affect *SY* (e.g., Dusar et al., 2011; Vanmaercke et al., 2015). Likewise, our variables do not account for spatial variations within the catchment that may also influence *SY* (e.g., de Vente et al., 2006, 2013).

However, a probably more important cause for these weak or counter-intuitive correlations are inter-correlations with other factors that have a stronger, 'overriding' effect on *SY* and may cause interactions (e.g., de Vente et al., 2013). In this respect, it is important to point out that our results are highly comparable to those of other studies focusing on *SY* at regional or continental scales. For example, also de Vente et al. (2011) and Vanmaercke et al. (2015) report very poor or even insignificant correlations between *SY* and land use for catchments in Spain and Europe, respectively. They attribute this to the fact that other controls exert a similar or larger control on *SY*, because, for example, agricultural catchments are often located in flatter areas and steep mountain catchments are often forested, both may have a similar *SY* (Vanmaercke et al., 2015). Likewise, as Vanmaercke et al. (2014c) showed for Romania, inter-correlation between topography and lithology and seismicity (i.e., steeper catchments consist of stronger rocks and have fewer earthquakes) may result in a negative correlation between average catchment slope and *SY*. This is highly similar to what we observe here (**Table 3**, **Figs. 3** and **4**). For similar reasons, many studies indicate only weak or

even insignificant correlations between *SY* and climatic factors at regional, continental or global scales (Aalto et al., 2006; Syvitski and Milliman, 2007; de Vente et al., 2011; Vanmaercke et al., 2014a,b, 2015), which also corresponds with our results (**Table 3**, **Fig. 3d**).

It is outside the scope of this paper to fully disentangle all these correlations and factors controlling *SY* across Italy. As indicated in the Introduction, we statistically explore the degree of correlation between *SY* and different measures of seismic and tectonic activity in order to better understand the mechanisms behind previously observed correlations between seismicity and *SY*. In this context, we considered non-tectonic factors to ensure that our results are not biased by other factors controlling *SY*.

The degree of correlation between *SY* and our tectonic proxies varied greatly (**Table 3**, **Figs. 4 and 5**). These differences and their implications will be discussed below. At this point, however, it is important to point out that seismicity overall shows a highly significant correlation with *SY* (**Fig. 4**). Some of the weaker correlations between *SY* and seismic proxies (i.e., mainly those relating to rare but large earthquakes) became insignificant after controlling for inter-correlations with other factors (e.g., lithology and climate). However, for many of the other seismic proxies, our analyses showed that seismicity is significantly correlated to *SY* and that this correlation cannot be attributed to biases caused by the *SY* measuring method or the presence of upstream reservoirs, nor to inter-correlations with other factors controlling *SY*. This corresponds to our expectations and closely agrees with other recent studies reporting significant correlations between *SY* and seismicity in Taiwan (Dadson et al., 2003), Europe (Vanmaercke et al., 2014a), Africa (Vanmaercke et al., 2014b), Romania (Vanmaercke et al., 2014c), And worldwide (Portenga and Bierman, 2011; Vanmaercke et al., 2014a).

4.2. Role of tectonic uplift

As discussed in the introduction, previously observed correlations between *SY* and proxies of seismicity might be attributed to the fact that tectonic uplift often correlates with seismicity, while the river incision and topographic steepening resulting from this uplift causes the increase in sediment fluxes. While this is certainly a highly relevant mechanism in various rapidly uplifting environments (e.g., Montgomery and Brandon, 2002; DiBiasi et al., 2010; Larsen and Montgomery, 2012), our results for Italy do not immediately concur with this.

Firstly, our proxies of seismicity are negatively correlated to our proxies of tectonic uplift (**Table 3**, **Fig. 1**). This indicates that, at least in Italy, the currently most strongly uplifting

regions do not coincide with the most seismically active ones. In addition, we observed a negative correlation between contemporary vertical ground motion rates and *SY* (**Fig. 4a**). This is attributable to the fact that VD_{avg} correlates negatively to both *L* and seismicity, which both show highly significant positive correlations with *SY* (**Table 3**).

Evidently, these findings should be interpreted with caution since both the *SY* data and the ground velocity rates are subject to important uncertainties. Likewise, the actual response of rivers systems to tectonically induced base level changes are often highly complex (e.g., Tucker and Hancock, 2010; DiBiasi et al., 2010) and may not be fully reflected by the variables considered here. Nonetheless, our results strongly suggest that contemporary uplift rates and resulting river incision do not exert a first order control on contemporary *SY* in Italy. The fact that average catchment slope (a direct proxy for topographic steepness, which is also positively correlated to VD_{avg}; **Table 3**) correlates negatively with *SY* (**Fig. 3a**) supports this inference.

It is important to note that our results do not imply that contemporary tectonic movements and resulting river incision have no influence on *SY* in Italy. As case studies indicate, river incision may exert a strong control on patterns of landsliding in some Italian regions (e.g., Borgomeo et al., 2014). It is also likely that more detailed analyses (e.g., based on river profiles) would reveal an influence of tectonic uplift and river incision on *SY*. We wish only to indicate that tectonic uplift shows no positive correlation with *SY*, nor does it positively correlate with seismicity. Hence, the observed correlations between seismicity and *SY* across Italy are most likely not attributable to mechanisms of tectonic uplift and river incision alone.

4.3. Large versus small earthquakes and their link with landslides

A key finding of our work is that measures related to relatively weak but frequent seismicity (e.g., $CSM_{2\text{-}3}$, $CSM_{3\text{-}4}$, and $CSM_{2\text{-}4}$) show a higher degree of correlation than measures related to large but infrequent earthquakes (e.g., $CSM_{5\text{-}6}$, CSM_{6+}, and $CSM_{4\text{-}8}$; **Fig. 5**). Also expected *PGA* values associated with shorter recurrence intervals (and hence lower earthquake magnitudes) exhibit a slightly stronger correlation with *SY* than those associated with longer observation periods (**Fig. 5**). A first reason might be that the number of large earthquakes is limited, making the spatial pattern over a relatively short time period (i.e., 1900–2014) more erratic. This, combined with the uncertainties associated with the geographical distribution of the seismic energy release (**Section 2.1**), and the fact that the timing of the large earthquakes does not always concur with the measuring periods of the *SY* data, can result in low

correlations. We expect a better agreement between *SY* and *CSM* of large earthquakes that occurred during or just before the *SY* measuring period. Testing this was impossible in this study, due to the difference in the observation periods for earthquakes and *SY*.

Nonetheless, uncertainties and discrepancies in the observation periods also affect the correlations between *SY* and *CSM* values associated with smaller ($2 \leq M_w < 4$) earthquakes, which are stronger. Likewise, such uncertainties cannot account fully for the consistent decrease observed in **Fig. 5**. Hence, our results indicate that weak but frequent seismicity exerts a larger influence on regional patterns of *SY* on decadal time scales than large but infrequent earthquakes. Studies that did research the impacts of large earthquakes on catchment sediment export seem to confirm this. For example, Hovius et al. (2011) quantified the impact of the M_w 7.6 Chi-Chi earthquake in Taiwan on the sediment transport of river systems near the epicenter. It was estimated that suspended sediment export increased with a factor 5 to 6 in the year following the earthquake, due to the effects of earthquake-triggered landslides. However, this increase progressively declined during the following 6 to 7 years. As a result, the direct impact of this event on long-term average *SY* over a period of e.g., 20 years would be only in the order of a factor of two. Although this can still be considered significant, it is a relatively limited increase when compared to the range of average *SY* values at regional and continental scales (e.g., the *SY* values of this study vary over more than three orders of magnitude; **Figs. 3** and **4**). Likewise, Vanmaercke et al. (2014c) found that a M_w 7.4 earthquake in the Sub Carpathians (Romania) generally did not result in a significant increase of sediment export of catchments near the epicenter. This indicates that not all large earthquakes directly influence *SY*. Nevertheless, Vanmaercke et al. (2014c) did find very high correlations between average *SY* and expected *PGA*, showing that seismicity does have a significant impact on average *SY*. Given the fact that expected *PGA* is highly correlated to the occurrence of small earthquakes (Turcotte and Malamud, 2004; **Table 3**), we conclude that the impacts of seismicity on *SY* is mainly indirect, and we attribute it to the role of weak but frequent seismicity.

Landslides likely play an important role in the influence of seismicity on *SY*. Whereas we found a highly significant correlation between *SY* and *L*, which provides a first order proxy for landslide susceptibility (**Fig 3b**), previous studies also have highlighted the importance of landsliding on *SY* (de Vente et al., 2006, 2013). Our results (**Figs. 6** and **7**) show that landslides within a lithological unit are more likely to occur in regions of weak but frequent seismicity (M_w 2–4). Although only larger earthquakes ($M_w > 4$) are expected to directly

trigger landslides (Keefer, 2002; Malamud et al., 2004), the correlations between landslide patterns and $CSM_{4\text{-}8}$ were much lower. This indicates that the most important geomorphic effects of seismicity do not necessarily directly trigger landslides. Seismicity mainly plays a role as preparatory factor for landsliding, whereas the actual landslide may be triggered by other events such as heavy rainfall. Several other recent studies have pointed to the importance of indirect impacts of seismicity on landsliding (e.g., Huang et al., 2013; Marc et al., 2015; Carlini et al. 2016; Bucci et al., 2016). Furthermore, some very large earthquakes are known to have triggered only a very limited number of landslides (e.g., Jibson et al., 2006). These findings have important implications for our understanding of landslide hazards and risk, as seismicity is often considered only as a triggering factor for landslides, and not as a predisposing factor that increases landslide susceptibility (e.g., Huang et al., 2013; Jaedicke et al., 2014; Günther et al., 2014). Our results imply that this is incorrect. Nonetheless, the overall importance of seismicity as a factor influencing landslide susceptibility remains poorly understood. For example, **Figs. 6** and **7** show that the degree of spatial correlation between *LS* and seismicity varies greatly between the considered lithological units. To some extent, this may be attributed to the role of other factors (e.g., topography and rainfall). However, also the lithological characteristics can play an important role, as some lithological types are more easily fractured than others. At first sight, correlations between $CSM_{2\text{-}4}$ and *LF* indeed tend to increase with lithological weakness (**Fig. 7**, **Table 2**). However, there are also important exceptions to this tendency such as intrusive rocks, turbidites, and chaotic mélange (**Fig. 7**). Explaining these differences was outside the scope of this research and requires a different research set up. Nevertheless, this matter certainly deserves further research.

5. Conclusions

We found significant correlations between spatial patterns of seismicity and average catchment sediment yield (*SY*) across Italy. This is in agreement with other recent studies (Portenga and Bierman, 2011; Vanmaercke et al., 2014a,b,c). At least three mechanisms may explain these correlations between seismicity and *SY*: inter-correlations between seismicity and tectonic uplift, earthquake-triggered landsliding, and lithological weakening due to frequent seismicity. Our results suggest that, across Italy, especially this last mechanism is important. Firstly, *SY* shows highly significant correlations with proxies of weak but frequent seismicity that cannot be attributed to inter-correlations with other factors (**Table 3**, **Fig. 4d**), while proxies relating to large infrequent earthquakes showed much weaker correlations that overall became insignificant after controlling for inter-correlations with other factors (**Fig. 5**).

Proxies of tectonic uplift even showed a negative correlation with *SY* due to inter-correlations with other factors (**Fig. 4a**). In addition, spatial patterns of the known landslides in a given lithological type showed a significant positive correlation with proxies of weak seismicity, while this was not the case for proxies relating to large earthquakes (**Figs. 6 and 7**).

These findings do not imply that tectonic uplift or large landslide-triggering earthquakes have no influence on *SY* in Italy. Nonetheless, we argue that their influence on regional patterns of *SY* on a decadal timescale is much smaller than the effect of weak but frequent seismicity. This has important implications for our understanding of geomorphic processes on regional and continental scales, as the effects of weak but frequent seismicity are rarely considered (Cox et al., 2010; de Vente et al., 2013; Vanmaercke et al., 2014a). Also for landslide risk assessments, these findings are highly relevant as they indicate that seismicity should be considered not only as a triggering but also as a preparatory factor of landslides.

Acknowledgment

M. Vanmaercke acknowledges the financial support from the Research Foundation Flanders (FWO). We thank Enrico Serpelloni (INGV) for kindly providing data on vertical ground velocities in Italy. We also thank the two anonymous reviewers for their constructive comments.

References

Aalto, R., Dunne, T., Guyot, J., 2006. Geomorphic controls on Andean denudation rates. J. Geol. 114, 85–99.

APAT, 2007. Rapporto sulle frane in Italia: il progetto IFFI, metodologia, resultati e rapporti regionali. Rapporto 78/2007. Agenzia per la Protezione dell'Ambiente e per i Servizi Tecnici, Rome, Italy.

Bindi, D., Luzi, L., Pacor, F., Sabetta, F., Massa, M., 2009. Towards a new reference ground motion prediction equation for Italy: update of the Sabetta–Pugliese (1996). Bulletin of Earthquake Engineering, 7(3), 591-608.

Borgomeo, E., Hebditch, K. V., Whittaker, A. C., Lonergan, L., 2014. Characterising the spatial distribution, frequency and geomorphic controls on landslide occurrence, Molise, Italy. Geomorphology, 226, 148-161.

Bucci, F., Santangelo M., Cardinali M., Fiorucci F., Guzzetti F. (2016) Landslide distribution and size in response to Quaternary fault activity: the Peloritani Range, NE Sicily, Italy. Earth Surface Processes and Landforms 41, 711-720.

Cardinali, M. Guzzetti F., Santangelo M., 2013. Valutazione Euristica della Pericolosità da Frana per le Zone di Allerta di Protezione Civile. Technical Report, 1455 pp. (in Italian).

Carlini, M., Chelli, A., Vescovi, P., Artoni, A., Clemenzi, L., Tellini, C., Torelli, L., 2016. Tectonic control on the development and distribution of large landslides in the Northern Apennines (Italy). Geomorphology, 253, 425-437.

CGIAR, 2008. SRTM 90 m digital elevation data. Available online, http://srtm.csi.cgiar.org/ (last accessed: 17 December 2015).

Cox, R., Zentner, D.B., Rakotondrazafy, A.M.F., Rasoazanamparany, C.F., 2010. Shakedown in Madagascar: occurrence of lavakas (erosional gullies) associated with seismic activity. Geology 38, 179–182.

Dadson, S.J., Hovius, N., Chen, H., Dade, W.B., Hsieh, M.-L.,Willet, S.D., Hu, J.-C., Horng,M.-J., Chen, M.-C., Stark, C.P., Lague, D., Lin, J.-C., 2003. Links between erosion, runoff variability and seismicity in the Taiwan orogen. Nature 426, 648–651.

Dusar, B., Verstraeten, G., Notebaert, B., Bakker, J., 2011. Holocene environmental change and its impact on sediment dynamics in the Eastern Mediterranean. Earth Sci. Rev. 108, 137–157.

de Vente, J., Poesen, J., Bazzoffi, P., Van Rompaey, A., Verstraeten, G., 2006. Predicting catchment sediment yield in Mediterranean environments: the importance of sediment sources and connectivity in Italian drainage basins. Earth Surface Processes and Landforms, 31, 1017–1034.

de Vente, J., Verduyn, R., Verstraeten, G., Vanmaercke, M., Poesen, J., 2011. Factors controlling sediment yield at the catchment scale in NW Mediterranean geoecosystems. J. Soils Sediments 11, 690–707.

de Vente, J., Poesen, J., Verstraeten, G., Govers, G., Vanmaercke, M., Van Rompaey, A., Arabkhedri, M., Boix-Fayos, C., 2013. Predicting soil erosion and sediment yield at regional scales: where do we stand? Earth Science Review, 127, 16–29.

DiBiasi, R.,Whipple, K., Heisath, A., Ouimet,W., 2010. Landscape form and millennial erosion rates in the San Gabriel Mountains, CA. Earth Planet. Sci. Lett. 289, 134–144.

EEA, 2010. Corine Land Cover 1990 raster data — version 13 (02/2010). Available online: http://www.eea.europa.eu/data-and-maps/data/corine-land-cover-1990-raster (last accessed: 17 December 2015).

Fekete, B.M., Vörösmarty, C.J., Grabs,W., 1999. Global composite runoff fields on observed river discharge and simulated water balances. Federal Institute of Hydrology (BfG) - Global Runoff Data Centre (GRDC), Koblenz (Report 22).

Ferro, V., Di Stefano, C., Minacapilli, M., Santoro, M., 2003. Calibrating the SEDD model for Sicilian ungauged basins. In: De Boer, D., Froehlich, W., Mizuyama, T., Pietroniro, A. (Eds.), Erosion Prediction in Ungauged Basins: Integrating Methods and Techniques (Proceedings of SymposiumHS01HeldDuring IUGG2003 at Sapporo, July 2003). IAHS Publ., 279. IAHS, Wallingford, United Kingdom, pp. 151–161.

Fisher, R.A., 1924. The distribution of the partial correlation coefficient. Metron 3, 329–332.

Gazzolo, T., Bassi, G., 1960. Contribution a létude du dégré dérosion des sols constituant les bassins versant des cours d'eau Italiens. Proceedings of the General Assembly of Helsinki (25/7–6/8 1960). IAHS Publ., 53. IAHS, Gentbrugge, Belgium, pp. 112–134.

Günther, A., Van Den Eeckhaut, M., Malet, J. P., Reichenbach, P., Hervás, J., 2014. Climate-physiographically differentiated Pan-European landslide susceptibility assessment using spatial multi-criteria evaluation and transnational landslide information. Geomorphology, 224, 69–85.

Hovius, N., Meunier, P., Ching-Weei, L., Hongey, C., Yue-Gau, C., Dadson, S., Ming-Jame, H., Lines, M., 2011. Prolonged seismically induced erosion and the mass balance of a large earthquake. Earth and Planetary Science Letters 304, 347–355.

Huang, H.-P., Yang, K.-C., Lin, B.-W., 2013. Statistical evaluation of the effect of earthquake with other related factors on landslide susceptibility: using the watershed area of Shihmen reservoir in Taiwan as a case study. Environ Earth Sci, 69, 2151–2166.

ISIDE, 2015. Italian Seismological Instrumental and Parametric Data-base. Available online: http://iside.rm.ingv.it/iside/standard/index.jsp?page=faq (last accessed: 17 December 2015)

Jaedicke, C., Van Den Eeckhaut, M., Nadim, F., Hervás, J., Kalsnes, B., Vangelsten, B. V., et al., 2014. Identification of landslide hazard and risk 'hotspots' in Europe. Bulletin of Engineering Geology and the Environment, 73(2), 325–339.

Jibson, R. W., Harp, E. L., Schulz, W., Keefer, D. K., 2006. Large rock avalanches triggered by the M 7.9 Denali Fault, Alaska, earthquake of 3 November 2002. Engineering Geology, 83(1), 144–160.

Keefer, D.K., 1984. Landslides caused by earthquakes. Geological Society of America Bulletin 95, 406-421.

Keefer, D.K., 2002. Investigating landslides caused by earthquakes — a historical review. Surv. Geophys. 23, 473–510.

Keefer, D.K., 2013. Landslides Generated by Earthquakes: Immediate and Long-Term Effects. In: Shroder, J.F., Owen, L.A. (Eds.), Treatise on Geomorphology, vol. 5, Elsevier Ltd., San Diego, pp. 250–266.

Koi, T., Hotta, N., Ishigaki, I., Matuzaki, N., Uchiyama, Y., Suzuki, M., 2008. Prolonged impact of earthquake-induced landslides on sediment yield in a mountain watershed: The Tanzawa region, Japan. Geomorphology 101, 692-702.

Koons, P.O., Upton, P., Barker, A.D., 2012. The influence of mechanical properties on the link between tectonic and topographic evolution. Geomorphology 137, 168–180.

Larsen, I.J., Montgomery, D.R., 2012. Landslide erosion coupled to tectonics and river incision. Nat. Geosci. 5, 468–473.

Lehner, B., Verdin, K., Jarvis, A., 2006. Hydrological Data and Maps Based on Shuttle Elevation Derivatives at Multiple Scales (HydroSHEDS) - Technical Documentation.World Wildlife Fund U.S., Washington, DC, (27 pp. Available at: http://hydrosheds.cr.usgs.gov, accessed 22 August 2013).

Lenzi, M. A., Mao, L., Comiti, F., 2003. Interannual variation of suspended sediment load and sediment yield in an alpine catchment. Hydrological Sciences Journal, 48(6), 899-915.

Malamud, B.D., Turcotte, D.L., Guzzetti, F., Reichenbach, P., 2004. Landslides, earthquakes, and erosion. Earth Planet. Sci. Lett. 229, 45–59.

Marc, O., Hovius, N., Meunier, P., Uchida, T., Hayashi, S., 2015. Transient changes of landslide rates after earthquakes. Geology, 43(10), 883-886.

Marchesini, I., Ardizzone, F., Alvioli, M., Rossi, M., Guzzetti, F. 2014. Non-susceptible landslide areas in Italy and in the Mediterranean region. NHESS, 14(8), 2215–2231, doi:10.5194/nhess-14-2215-2014.

Meunier, P., Hovius, N., Haines, A.J., 2007. Regional patterns of earthquake-triggered landslides and their relation to ground motion. Geophysical Research Letters, 34(20).

Meunier, P., Hovius, N., Haines, A.J., 2008. Topographic site effects and the location of earthquake induced landslides. Earth Planet. Sci. Lett. 275, 221–232.

Meybeck, M., Ragu, A., 1995. River Discharges to the Oceans: an Assessment of Suspended Solids, Major Ions and Nutrients. U.N. Environment Programme (UNEP), Nairobi, Kenya. 240 pp.

Meybeck, M., 2003. Global analysis of river systems: from Earth system controls to Anthropocene controls. Philos. Trans. R. Soc. B 358, 1935–1955.

Moatar, F., Person, G., Meybeck, M., Coynel, A., Etcheber, H., Crouzet, P., 2006. The influence of contrasting suspended particulate matter transport regimes on the bias and precision of flux estimates. Sci. Total Environ. 370, 515–531.

Molnar, P., Anderson, R.S., Anderson, S.P., 2007. Tectonics, fracturing of rock, and erosion. J. Geophys. Res. 112, F03014. http://dx.doi.org/10.1029/2005JF000433.

Montgomery, D.R., Brandon, M.T., 2002. Topographic controls on erosion rates in tectonically active mountain ranges. Earth Planet. Sci. Lett. 201, 481–489.

New, M., Lister, D., Hulme, M., Makin, I., 2002. A high-resolution data set of surface climate over global land areas. Clim. Res. 21, 1–25.

Owens, P.N., Batalla, R.J., Collins, A.J., Gomez, B., Hicks, D.M., Horowitz, A.J., Kondolf, G.M., Marden, M., Page, M.J., Peacock, D.H., Petticrew, E.L., Salomons, W., Trustrum, N.A., 2005. Fine-grained sediment in River Systems: environmental significance and management issues. River Res. Appl. 21, 693–717.

Panagos, P., Meusburger, K., Ballabio, C., Borrelli, P., Alewell, C., 2014. Soil erodibility in Europe: A high-resolution dataset based on LUCAS. Science of the Total Environment, 479, 189-200.

Pavanelli, D., Rigotti, M., 2007. Relationship between suspended sediment concentration and total nitrogen, and comparison among basins for some Apennine Rivers. Proceedings of the COST 634 International Conference on Off-Site Impacts of Soil Erosion and Sediment Transport (1–3 October 2007). Czech Technical University in Prague, Faculty of Civil Engineering, Department of Drainage, Irrigation and Landscape Engineering, Prague, Czech Republic, pp. 167–176.

Pearce, A.J. & Watson, A.J., 1986. Effects of earthquake-induced landslides on sediment budget and transport over a 50-yr period. Geology 14, 52-55.

Phillips, J.,Webb, B.,Walling, D., Leeks, G., 1999. Estimating the suspended sediment loads of rivers in the LOIS study area using infrequent samples. Hydrol. Process. 13, 1035–1050.

Portenga, E.W., Bierman, P.R., 2011. Understanding Earth's eroding surface with 10Be. GSA Today 24. http://dx.doi.org/10.1130/G111A.1.

Rovida, A., Camassi, R., Gasperini, P., Stucchi, M. (Eds.), 2011. CPTI11, the 2011 version of the Parametric Catalogue of Italian Earthquakes. Istituto Nazionale di Geofisica e Vulcanologia, Milano, Bologna, http://emidius.mi.ingv.it/CPTI, doi:10.6092/INGV.IT-CPTI11

Scordilis, E. M., 2006. Empirical global relations converting M S and m b to moment magnitude. Journal of Seismology, 10(2), 225-236.

Selvaggi, G., Castello, B., Azzara, R., 1997. Spatial distribution of scalar seismic moment release in Italy (1983-1996): seismotectonic implications for the Apennines. Annals of Geophysics, 40(6), 1565-1578.

Serpelloni, E., Faccenna, C., Spada, G., Dong, D., Williams, S. D., 2013. Vertical GPS ground motion rates in the Euro-Mediterranean region: New evidence of velocity gradients at different spatial scales along the Nubia-Eurasia plate boundary. Journal of Geophysical Research: Solid Earth, 118(11), 6003-6024.

SHARE, 2013. European Facility for Earthquake Hazard and Risk – Seismic Hazard Maps. Available online: http://www.efehr.org:8080/jetspeed/portal/HazardMaps.psml (last accessed: 17 December 2015)

Sidle, R.C., Ochiai, H. 2006. Landslides: Processes, Prediction, and Land Use. Water Resources Monograph 18, American Geophysical Union, Washington D.C.

Steel, R.G.D., Torrie, J.H., 1960. Principles and Procedures of Statistics. McGraw-Hill, New York (672 pp.).

Syvitski, J.P.M., Milliman, J., 2007. Geology, geography, and humans battle for dominance over the delivery of fluvial sediment to the coastal ocean. J. Geol. 115, 1–19.

Tamburino, V., Barbagallo, S., Vella, P., 1990. Evaluation of sediment deposition in Sicilian artificial reservoirs. In: Sinniger, R., Monbaron, M. (Eds.), Hydrology in Mountainous Regions II: Artificial Reservoirs, Water and Slopes (Proceedings of Two Lausanne

Symposia, August 1990). IAHS Publ., 194. IAHS, Wallingford, United Kingdom, pp. 107–112.

Torri, D., Borselli, L., Guzzetti, F., Calzolari, M.C., Bazzofi, P., Ungaro, F., Bartolini, D., Salvador Sanchis, M.P., 2006. Italy. In: Boardman, J., Poesen, J. (eds.), Soil Erosion in Europe. John Wiley and Sons Ltd., Chichester, United Kingdom, pp. 245–262.

Trigila, A., Iadanza, C., Spizzichino, D., 2010. Quality assessment of the Italian Landslide Inventory using GIS processing. Landslides, 7(4), 455-470.

Tropeano, D., 1984. Soil loss and sediment yield from a small basin in the Langhe area, Piedmont (NW Italy): a first report. Geologia Applicata e Idrogeologica 19, 269–287.

Tucker, G.E., Hancock, G.R., 2010. State of science: Modelling landscape evolution. Earth Surface Processes and Landforms, 35, 28–50.

Turcotte, D.L., Malamud, B.D., 2004. Landslides, forest fires, and earthquakes: Examples of self-organized critical behaviour. Physica A, 340, 580–589.

Ufficio Idrografico e Mareografico, 1997. Presidenza del Consiglio dei Ministri, Serizi Tecnici Nazionali - Annali idrologici (1917-1997). (In Italian)

Vanmaercke, M., Poesen, J., Verstraeten, G., Maetens, W., de Vente, J., 2011a. Sediment yield as a desertification risk indicator. Sci. Total Environ. 409, 1715–1725

Vanmaercke, M., Poesen, J., Verstraeten, G., de Vente, J., Ocakoglu, F., 2011b. Sediment Yield in Europe: spatial patterns and scale dependency. Geomorphology 130, 142–161.

Vanmaercke, M., Poesen, J., Rădoane, M., Govers, G., Ocakoglu, F., Arabkhedri, M., 2012. How long should we measure? An exploration of factors controlling the interannual variation of catchment sediment yield. J. Soils Sediments 12, 603–619.

Vanmaercke, M., Kettner, J., Van Den Eeckhaut, M., Poesen, J., Mamaliga, A., Verstraeten, G., Radoane, M., Obreja, F., Upton, P., Syvitski, J., Govers, G., 2014a. Moderate seismic activity affects contemporary sediment yields. Prog. Phys. Geogr. 38, 145–172.

Vanmaercke, M., Poesen, J., Broeckx, J., Nyssen, J., 2014b. Sediment yield in Africa. Earth-Science Reviews, 136, 350-368.

Vanmaercke, M., Obreja, F., Poesen, J., 2014c. Seismic controls on contemporary sediment export in the Siret river catchment, Romania. Geomorphology, 216, 247–262.

Vanmaercke, M., Poesen, J., Govers, G., Verstraeten, G., 2015. Quantifying human impacts on catchment sediment yield: A continental approach. Global and Planetary Change, 130, 22-36.

Van Rompaey, A., Bazzoffi, P., Jones, R.J.A., Montanarella, L., 2005. Modelling sediment yields in Italian catchments. Geomorphology, 65, 157–169.

Verstraeten, G., Poesen, J., 2002. Using sediment deposits in small ponds to quantify sediment yield from small catchments: possibilities and limitations. Earth Surface Processes and Landforms, 27, 1425–1439.

TABLES

Table 1. Variables considered to investigate the observed differences in sediment yield (*SY*) in 103 catchments in Italy (**Figs. 1 and 2**).

Variable	Factor	Description	Source	Range	Units
MeasType	Measuring Procedure	Dummy variable indicating if SY was calculated from gauging station observations (0) or from reservoir sedimentation rates (1)	Source of the *SY* data	0 or 1	/
A	Size	Drainage area of the catchment	Source of the *SY* data	5-6075	km²
UpRes	Reservoir Impacts	Dummy variable indicating if the SY was potentially significantly affected by upstream reservoirs (0) or not (1)	Source of the *SY* data, Google Earth	0 or 1	/
P	Climate	Average (1961-1990) annual rainfall	New et al. (2002)	427 - 1832	mm y^{-1}
RDN	Climate	Average (1961-1990) rainy day normal (i.e. P divided by the average number of days per year with rain)	New et al. (2002)	3.9 - 9.6	mm day^{-1}
T	Climate	Average (1961-1990) air temperature	New et al. (2002)	-1.3 - 17.0	° C
Ro	Climate	Estimated annual runoff depth, based on observed river discharges and simulated water balances	Fekete et al. (1999)	34 - 2172	mm y^{-1}

S_{avg}	Topography	Average catchment slope, derived from SRTM data (spatial resolution ~81 m)	CGIAR (2008)	1.6 - 30.5	°
Kst	Lithology/Soil	Average soil erodibility of the catchment, as defined in the (Revised) Universal Soil Loss equation and accounting for stoniness	Panagos et al. (2014)	0.017 - 0.041	(t ha h) / (ha MJ mm)
L	Lithology/Soil	Susceptibility of the lithology for landsliding (see text)	Cardinali et al. (2013)	0.01 - 0.20	/
AL	Land cover	Percentage of the catchment used for agriculture, acccording to the Corine land cover dataset of 1990	EEA (2010)	0 - 99	%
FOREST	Land cover	Percentage of the catchment covered by forests, acccording to the Corine land cover dataset of 1990	EEA (2010)	0 - 98	%
VD_{avg}	Tectonics	Average estimated annual vertical ground motion rate of the catchment	Serpelloni et al. (2013)	-2.9 - 1.7	mm y^{-1}
VD_{min}	Tectonics	Minimum estimated annual vertical ground motion rate in the catchment	Serpelloni et al. (2013)	-4.8 - 1.5	mm y^{-1}
VD_{max}	Tectonics	Maximum estimated annual vertical ground motion rate in the catchment	Serpelloni et al. (2013)	-1.8 - 2.3	mm y^{-1}

VD_{range}	Tectonics	Difference between VD_{max} and VD_{min}, divided by the drainage area of the catchment	Serpelloni et al. (2013)	0.0004 - 0.03	mm y^{-1} km^{-2}
PGA_{73y}	Tectonics	Estimated maximum Peak Ground Acceleration expected to occur with a recurrence interval of 73 years (average value of the catchment)	SHARE (2013)	0.0077 - 0.14	g
PGA_{102y}	Tectonics	Estimated maximum Peak Ground Acceleration expected to occur with a recurrence interval of 102 years (average value of the catchment)	SHARE (2013)	0.010 - 0.18	g
PGA_{475y}	Tectonics	Estimated maximum Peak Ground Acceleration expected to occur with a recurrence interval of 475 years (average value of the catchment)	SHARE (2013)	0.0334 - 0.39	g
PGA_{975y}	Tectonics	Estimated maximum Peak Ground Acceleration expected to occur with a recurrence interval of 975 years (average value of the catchment)	SHARE (2013)	0.056 - 0.54	g
PGA_{2475y}	Tectonics	Estimated maximum Peak Ground Acceleration	SHARE (2013)	0.12 - 0.85	g

		expected to occur with a recurrence interval of 2475 years (average value of the catchment)			
PGA_{4975y}	Tectonics	Estimated maximum Peak Ground Acceleration expected to occur with a recurrence interval of 4975 years (average value of the catchment)	SHARE (2013)	0.17 - 1.1	g
CSM_{All}	Tectonics	Cumulative seismic moment of all considered earthquakes (see section 2.1)	See text	96.8 - 924.2	10^{10} N m y^{-1}
CSM_{2-4}	Tectonics	Cumulative seismic moment of all considered earthquakes with a magnitude between 2 and 4 (see section 2.1)	See text	2.6 - 14.7	10^{10} N m y^{-1}
CSM_{4-8}	Tectonics	Cumulative seismic moment of all considered earthquakes with a magnitude greater than 4 (see section 2.1)	See text	93.8 - 917.9	10^{10} N m y^{-1}
CSM_{2-3}	Tectonics	Cumulative seismic moment of all considered earthquakes with a magnitude between 2 and	See text	1.2 - 8	10^{10} N m y^{-1}

		3 (see section 2.1)			
$CSM_{3\text{-}4}$	Tectonics	Cumulative seismic moment of all considered earthquakes with a magnitude between 3 and 4 (see section 2.1)	See text	1.4 - 6.7	10^{10} N m y^{-1}
$CSM_{4\text{-}5}$	Tectonics	Cumulative seismic moment of all considered earthquakes with a magnitude between 4 and 5 (see section 2.1)	See text	2.7 - 11.6	10^{10} N m y^{-1}
$CSM_{5\text{-}6}$	Tectonics	Cumulative seismic moment of all considered earthquakes with a magnitude between 5 and 6 (see section 2.1)	See text	13.8 - 85.2	10^{10} N m y^{-1}
CSM_{6+}	Tectonics	Cumulative seismic moment of all considered earthquakes with a magnitude greater than 6 (see section 2.1)	See text	70.3 - 868.7	10^{10} N m y^{-1}

Table 2. Lithological types considered in this study and their corresponding spatial extent, average slope and (normalized) landslide fractions. The lithological classification and its mapping was derived from Cardinali et al. (2013).

Lithological unit	Spatial extent (km²)	Average slope (°)	Landslide fraction	Slope-normalized landslide fraction
Aeolian deposits	1688	1.5	0.000	0.001
Basalts	60	8.7	0.005	0.006
Intrusive rocks	9799	13.7	0.011	0.009
Lavas and Ignimbrites	17181	8.6	0.010	0.013
Carbonate rocks	56720	15.1	0.024	0.017
None-Schist metamorphic rocks	8163	23.0	0.042	0.019
Shales and Shists	16820	21.7	0.052	0.025
Alluvial deposits	73118	2.1	0.005	0.026
Ophiolites	3350	21.1	0.065	0.032
Glacial deposits	3488	13.4	0.050	0.039
Lacustrine deposits	5524	7.0	0.031	0.046
Clastic sediments	26438	9.0	0.056	0.064
Marls	6603	12.1	0.076	0.065
(Complex) clay layers	17447	7.7	0.062	0.084
Turbidites	49014	12.7	0.104	0.085
Chaotic Melange	2749	11.3	0.289	0.266
Italy	301212	10.4	0.042	-

Table 3. Spearman rank correlation coefficient matrix between all considered catchment characteristics (**Table 1**) and the observed catchment sediment yield (*SY*). Values in bold are highly significant ($p < 0.0001$) and values in italic are not significant ($p > 0.05$). Correlations were calculated for the 103 selected catchments (**Fig. 1**).

	MeasType	*A*	*UpRes*	*P*	*RDN*	*T*	*Ro*	S_{avg}	*Kst*	*L*	*AL*	*FOREST*	VD_{avg}	VD_{min}	VD_{max}	VD_{range}	PGA_{73y}	PGA_{102y}	PGA_{475y}	PGA_{975y}	PGA_{2475y}	PGA_{4975y}	CSM_{All}	CSM_{2-4}	CSM_{4-8}	CSM_{2-3}	CSM_{3-4}	CSM_{4-5}	CSM_{5-6}	CSM_{6+}	*SY*
MeasType	1																														
A	**-.61**	1																													
UpRes	.23	-.36	1																												
P	*.18*	*-.12*	*.08*	1																											
RDN	*.18*	*-.18*	*.08*	**.70**	1																										
T	*-.19*	*.14*	*-.09*	**-.88**	**-.43**	1																									
Ro	.26	*-.10*	*.08*	**.58**	**.46**	**-.62**	1																								
S_{avg}	.22	*-.15*	*.05*	**.86**	**.53**	**-.89**	**.67**	1																							
Kst	*-.16*	*-.04*	*-.04*	*.05*	*-.04*	*.02*	*-.11*	*-.09*	1																						
L	-.20	*-.02*	*.24*	*-.16*	*-.04*	*.10*	*-.19*	-.22	*.02*	1																					
AL	*.12*	-.20	*.06*	*.00*	*.16*	*.04*	*.00*	*-.03*	*.09*	*.09*	1																				
FOREST	*-.08*	.23	*-.13*	*-.06*	*-.15*	*.07*	*-.03*	*-.03*	*.00*	-.28	**-.61**	1																			
VD_{avg}	*.19*	*-.04*	*-.15*	*.19*	*-.08*	-.27	.20	.23	*.10*	**-.57**	*-.13*	*.15*	1																		
VD_{min}	**.52**	**-.43**	*.07*	*.18*	*.05*	-.24	.25	.24	*.01*	**-.50**	*.00*	*.06*	**.79**	1																	
VD_{max}	*-.09*	.29	-.24	*.12*	*-.16*	-.20	*.12*	*.12*	*.14*	**-.47**	-.24	.20	**.88**	**.46**	1																
VD_{range}	*.16*	**-.59**	.25	*.05*	*-.04*	*-.13*	*-.07*	*.06*	*.09*	.37	*.00*	*-.18*	*-.16*	*-.13*	*-.17*	1															
PGA_{73y}	-.24	.20	*.02*	-.22	*-.14*	*.13*	*.01*	-.22	-.24	**.46**	*.00*	-.22	-.27	**-.45**	*-.06*	.27	1														
PGA_{102y}	-.24	.20	*.02*	-.22	*-.14*	*.13*	*.02*	-.22	-.25	**.45**	*.00*	-.22	-.27	**-.45**	*-.06*	.27	**1.00**	1													
PGA_{475y}	-.22	.21	*.01*	-.25	*-.16*	*.16*	*.02*	-.25	-.31	**.40**	*-.03*	*-.18*	-.25	**-.43**	*-.04*	.22	**.97**	**.98**	1												
PGA_{975y}	-.22	.22	*.00*	-.25	*-.16*	*.16*	*.01*	-.25	-.31	**.39**	*-.02*	*-.19*	-.25	**-.43**	*-.03*	.21	**.96**	**.97**	**1.0**	1											
PGA_{2475y}	-.22	.20	*.01*	-.28	*-.18*	.19	*-.04*	-.29	-.31	**.38**	*-.03*	*-.16*	-.24	**-.42**	*-.03*	.20	**.92**	**.93**	**.98**	**.99**	1										
PGA_{4975y}	-.22	.21	*.01*	-.28	*-.18*	.20	*-.05*	-.30	-.31	**.38**	*-.03*	*-.16*	-.24	**-.41**	*-.03*	*.19*	**.92**	**.93**	**.98**	**.98**	**1.00**	1									
CSM_{All}	*-.15*	*.12*	*-.14*	**-.61**	**-.45**	**.49**	-.27	**-.54**	-.32	*.15*	*.00*	*-.06*	*-.04*	*-.18*	*.07*	*.11*	**.65**	**.66**	**.71**	**.71**	**.73**	**.73**	1								
CSM_{2-4}	-.36	.24	*-.03*	-.28	-.25	.21	*-.15*	-.30	*.03*	**.51**	*.03*	*-.19*	-.30	**-.56**	*-.05*	.33	**.84**	**.83**	**.79**	**.78**	**.76**	**.75**	**.59**	1							
CSM_{4-8}	*-.15*	*.12*	*-.15*	**-.62**	**-.45**	**.49**	-.28	**-.54**	-.32	*.15*	*.01*	*-.06*	*-.04*	*-.17*	*.07*	*.11*	**.64**	**.65**	**.70**	**.70**	**.73**	**.73**	**1.00**	**.58**	1						
CSM_{2-3}	-.36	.24	*-.02*	-.26	-.22	.20	*-.14*	-.29	*.04*	**.54**	*.04*	-.21	-.33	**-.57**	*-.08*	.33	**.83**	**.81**	**.77**	**.77**	**.74**	**.73**	**.56**	**.99**	**.55**	1					
CSM_{3-4}	**-.38**	.26	*-.02*	-.31	-.30	.24	*-.17*	-.33	*.00*	**.46**	*.00*	*-.16*	-.28	**-.55**	*-.02*	.32	**.84**	**.83**	**.80**	**.79**	**.77**	**.76**	**.63**	**.99**	**.62**	**.97**	1				
CSM_{4-5}	-.31	*.19*	*.03*	*-.10*	*-.10*	*.06*	*-.06*	*-.18*	*.01*	**.57**	*.05*	-.22	-.30	**-.53**	*-.07*	.36	**.80**	**.80**	**.76**	**.76**	**.74**	**.73**	**.51**	**.94**	**.50**	**.94**	**.91**	1			
CSM_{5-6}	**-.38**	.28	*-.04*	*.00*	-.23	*-.07*	*.02*	*-.07*	*.01*	.32	*-.05*	*-.12*	*-.11*	**-.47**	*.15*	.31	**.74**	**.74**	**.71**	**.71**	**.68**	**.67**	**.46**	**.86**	**.44**	**.83**	**.87**	**.81**	1		
CSM_{6+}	*-.12*	*.11*	*-.13*	**-.65**	**-.44**	**.53**	-.28	**-.57**	-.37	*.14*	*.01*	*-.06*	*-.05*	*-.14*	*.05*	*.07*	**.61**	**.62**	**.67**	**.68**	**.70**	**.71**	**.99**	**.52**	**.99**	**.49**	**.56**	**.45**	.36	1	
SY	*-.16*	*.19*	*.02*	-.32	*-.19*	.33	-.28	-.34	*.10*	**.44**	*-.06*	*-.09*	-.30	**-.40**	*-.15*	*.14*	.35	.34	.33	.33	.31	.29	.26	**.44**	.25	**.44**	**.43**	.35	.29	.23	1

FIGURE CAPTIONS

Fig. 1. Location of the 103 catchments in Italy with an average measured sediment yield (*SY*) value, and for which the drainage area could be delineated accurately using GIS.

Fig. 2. Maps showing four of the included variables expressing tectonic and seismic activity and location of the considered catchments (black lines; **Fig. 1**). (a) Contemporary vertical displacement rate (*VD*), as estimated by Serpelloni et al. (2013). (b) Maximum expected Peak Ground Acceleration (*PGA*) expected to occur with a recurrence of 475 years (PGA_{475}; SHARE, 2013). (c) Cumulative Seismic Moment (*CSM*) of all selected earthquakes with $M_W > 2$, normalized for the timespan of the seismic record (CSM_{All}, **Section 2.1**). (d) *CSM* of all selected earthquakes with $2 < M_W < 4$, normalized for the timespan of the seismic record ($CSM_{2\text{-}4}$, **Section 2.1**).

Fig. 3. Scatterplots between observed catchment sediment yield (*SY*) and four non-tectonic characteristics (**Table 1**) for the selected 103 Italian catchments (**Fig. 1**). Regressions are based on the best working fit. R^2 indicates the corresponding coefficient of determination. (a) average catchment slope (S_{avg}) versus *SY*. (b) Estimated lithological susceptibility to landsliding (*L*) versus *SY*. (c) Percentage of the catchment covered by forest (*Forest*) versus *SY*. (*d*) Average air temperature (T_{avg}) versus *SY*.

Fig. 4. Scatterplots between observed catchment sediment yield (*SY*) and four tectonic characteristics for the selected 103 Italian catchments. See **Table 1** for an explanation of the variables. Regressions based on the best working fit. R^2 indicates the corresponding coefficient of determination.

Fig. 5. Spearman rank coefficients between observed catchment sediment yields (*SY*) and different measures of seismicity. (a) Correlation between *SY* and the average cumulative seismic moment (*CSM*) in the 103 catchments (**Fig. 1**) for different earthquake magnitudes. (b) Correlation between *SY* and the average estimated maximum peak ground acceleration (*PGA*) expected to occur within the indicated recurrence interval. See **Table 1** for an explanation of the variables. Values are listed in **Table 3**.

Fig. 6. Boxplots showing the distribution of cumulative seismic moments caused by earthquakes with (a) $2 < M_W < 4$ ($CSM_{2\text{-}4}$) and (b) $4 < M_W < 8$ ($CSM_{4\text{-}8}$) for all grid cells with landslides (LS) and with no landslides (NLS) in specific lithological types (**Table 2**). Only lithological types with at least 100 NLS and 100 LS grid cells are shown. A dark red box-plot indicates that the median cumulative seismic moment for LS cells is significantly higher than

NLS cells ($p < 0.05$) according to a Wilcoxon rank sum test. A light blue boxplot indicates that the median *CSM* value of NLS cells is significantly higher than that of LS cells significantly ($p < 0.05$). White boxplots indicate no significant difference.

Fig. 7. Spearman rank correlation coefficients (a) between the estimated cumulative seismic moments (*CSM*) and the fraction of each grid cell with mapped landslides (*LF*). Correlation coefficients are calculated based on all grid cells of a lithological type (**Table 2**). Blue bars show the correlation between *LF* and *CSM* for earthquakes with $2 < M_W < 4$ ($CSM_{2\text{-}4}$). Orange bars show correlation between *LF* and *CSM* for earthquakes with $4 < M_W < 8$ ($CSM_{4\text{-}8}$). Hatched bars show correlations that are not significant ($p > 0.05$). (b) Corresponding partial correlations after controlling for the average slope of each grid cell.

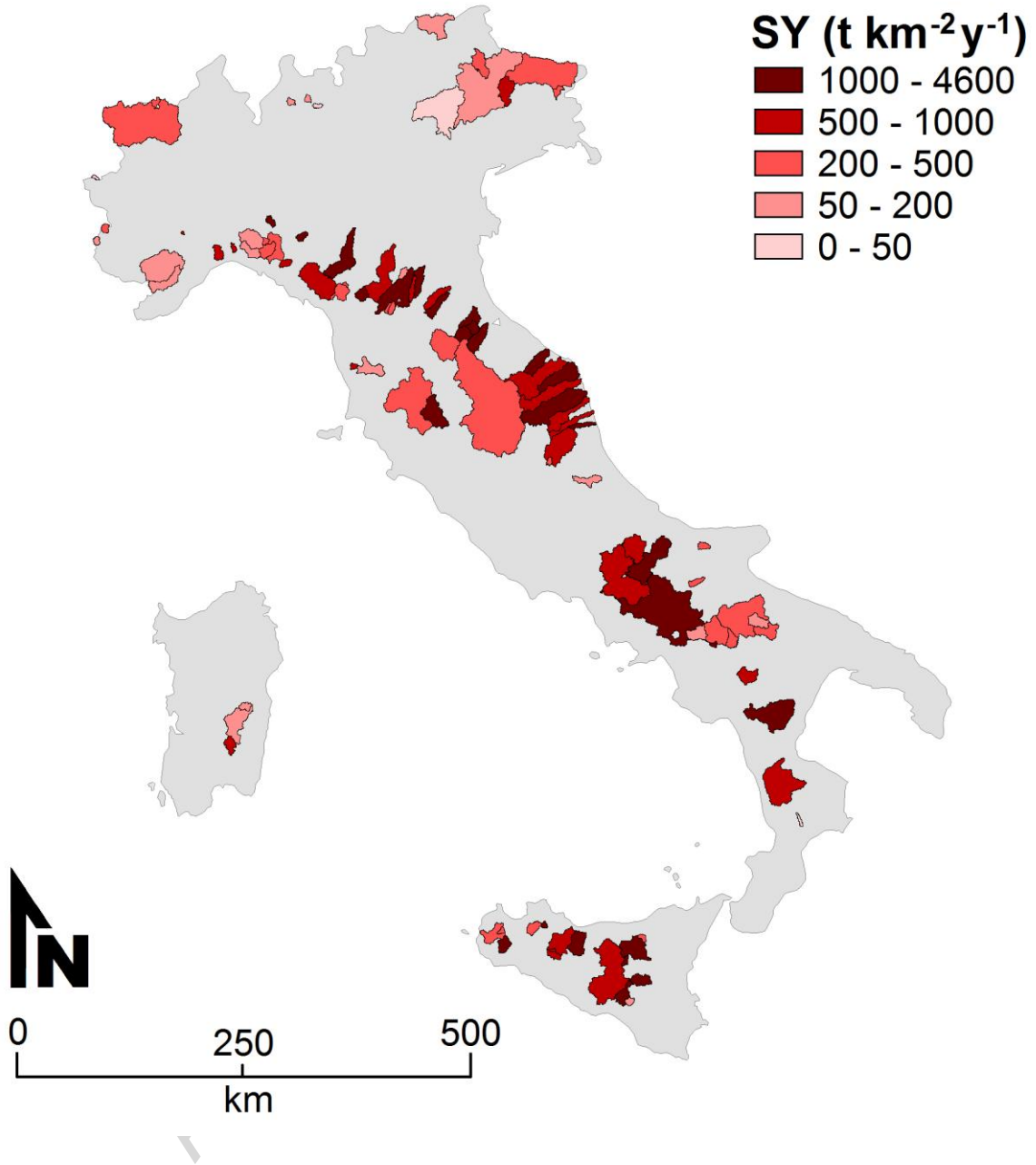

Fig. 1

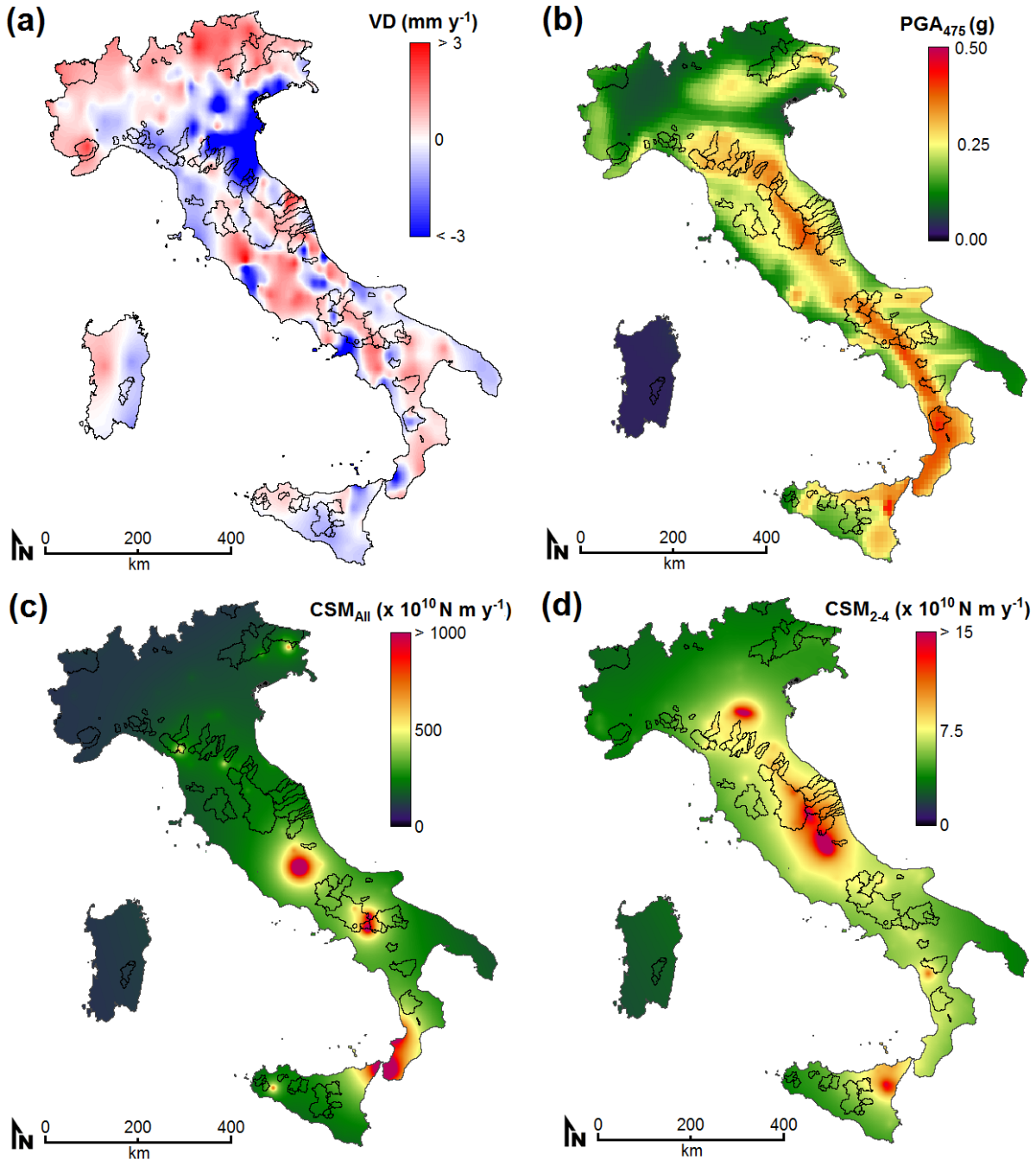

Fig. 2

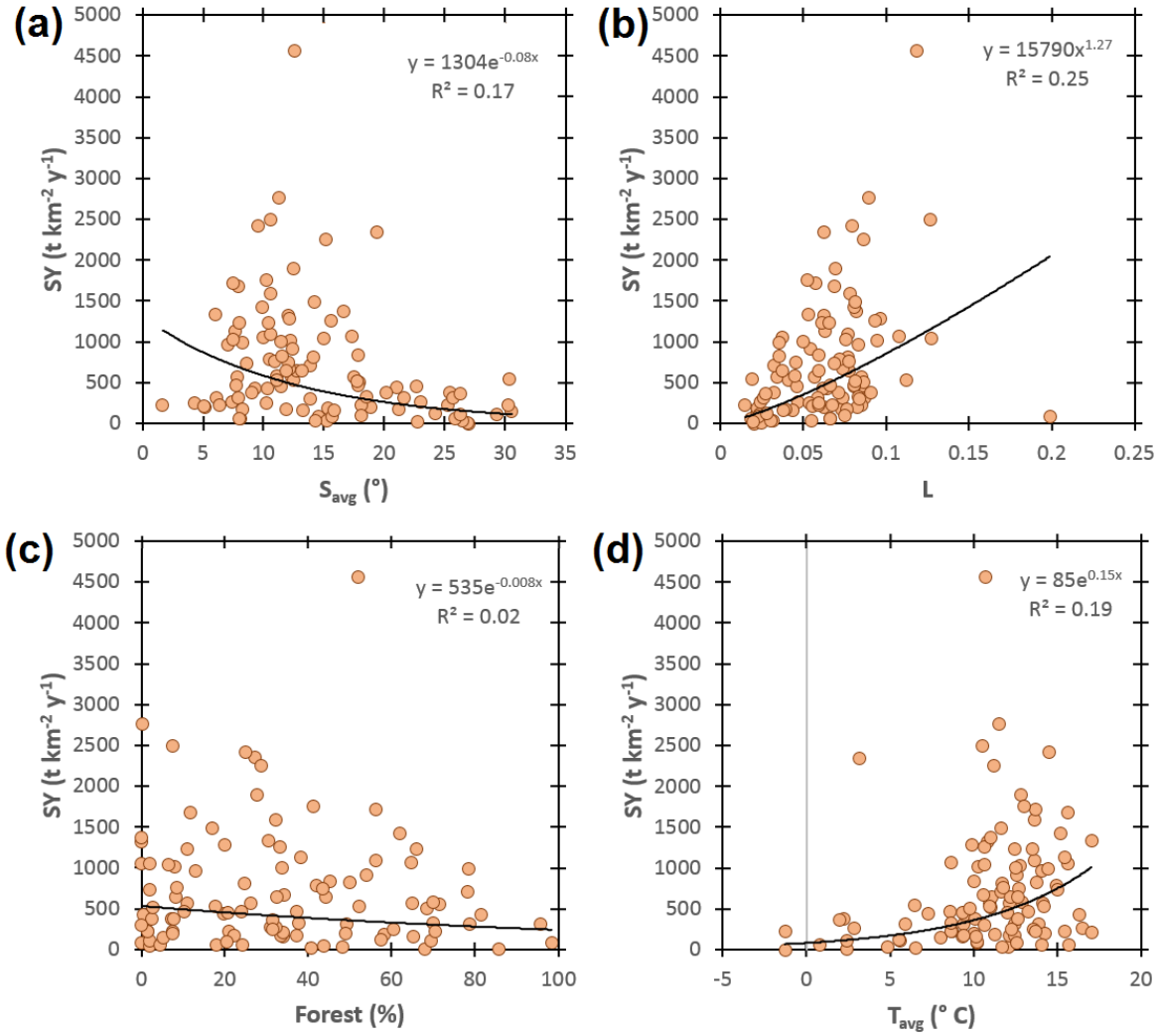

Fig. 3

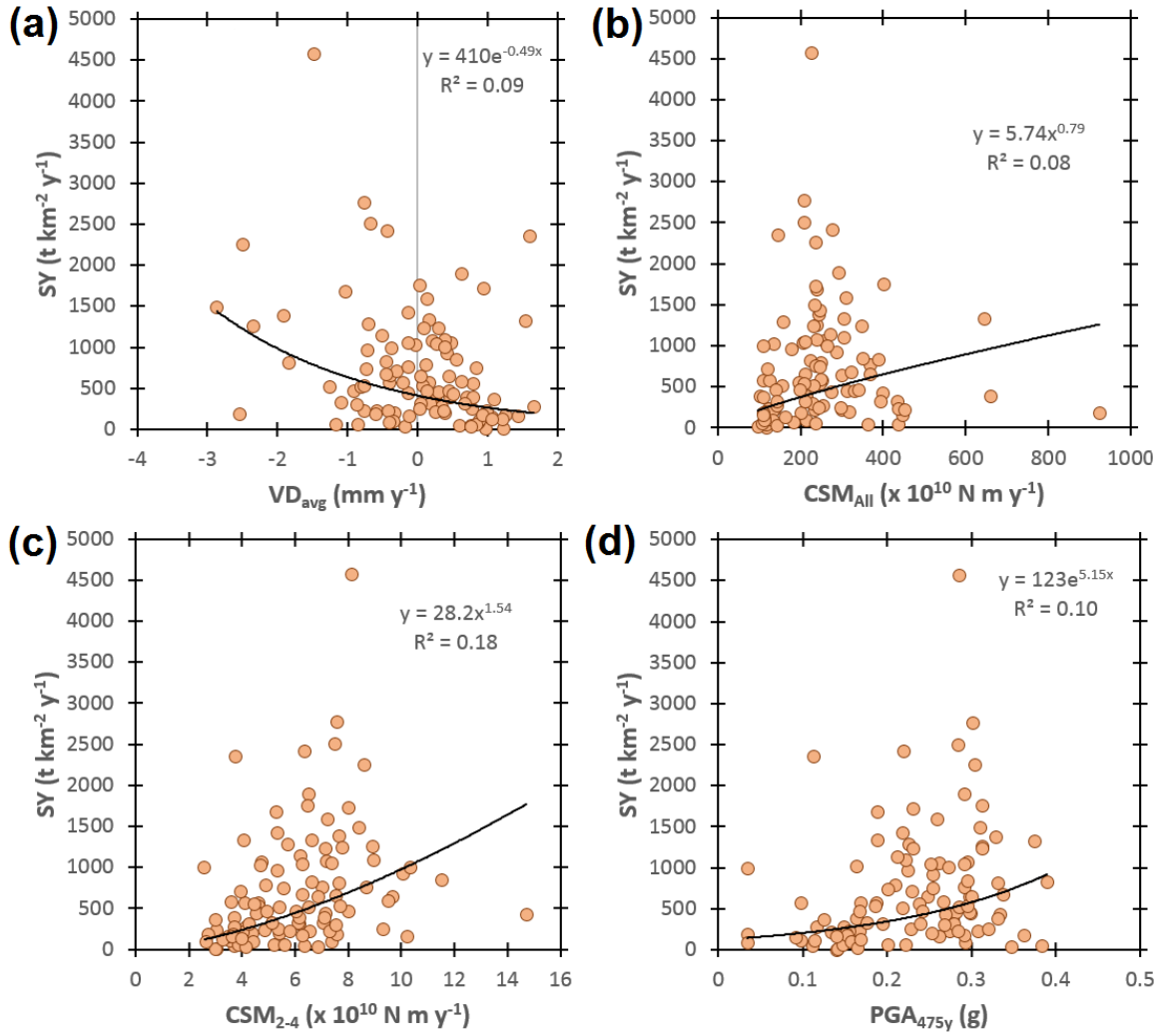

Fig. 4

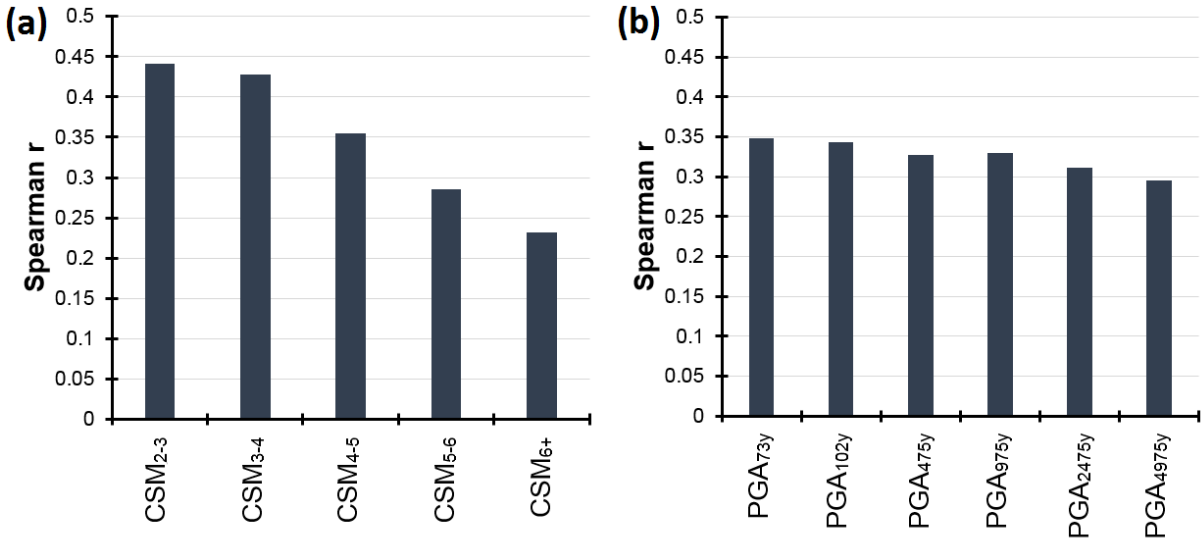

Fig. 5

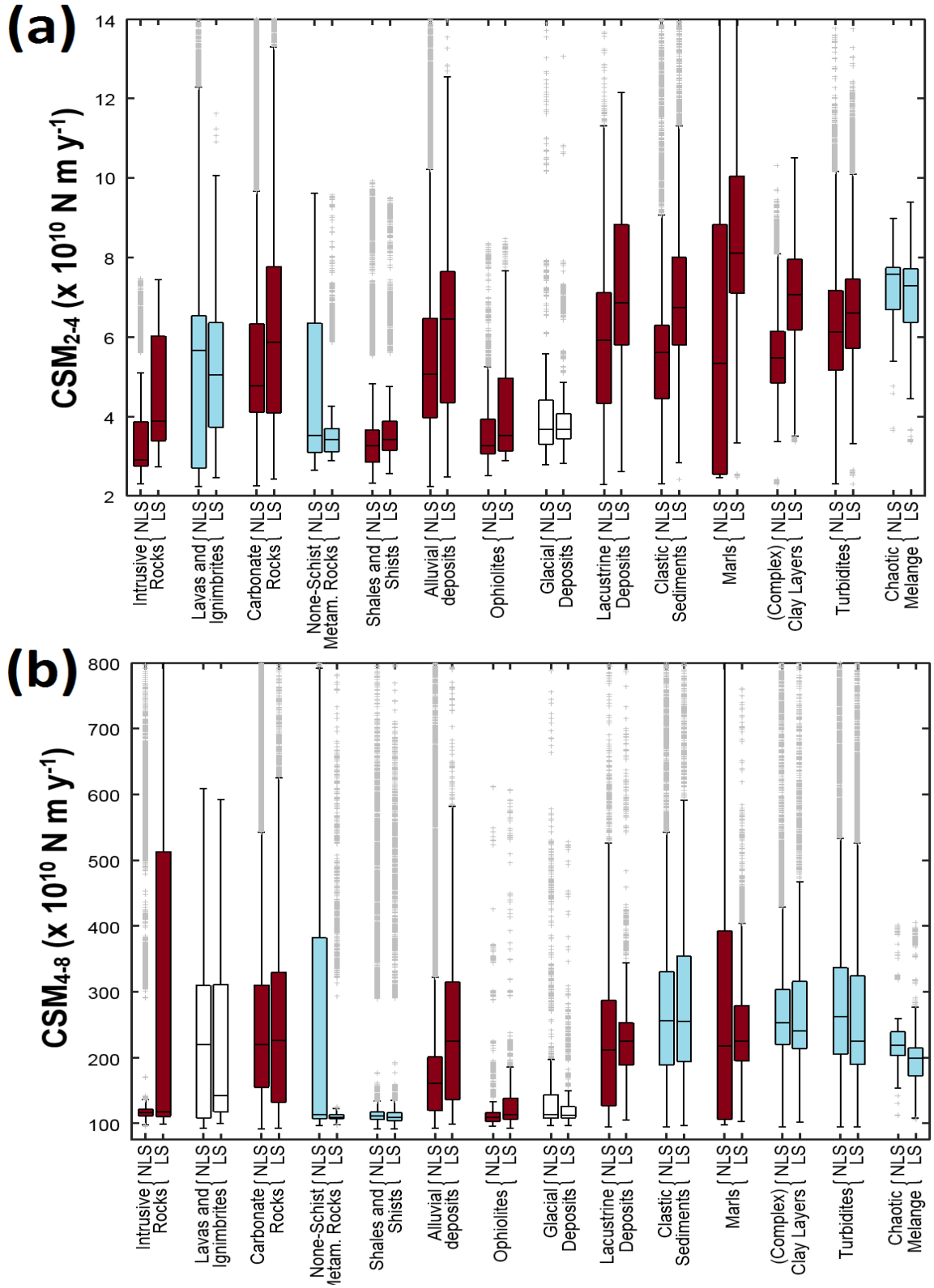

Fig. 6

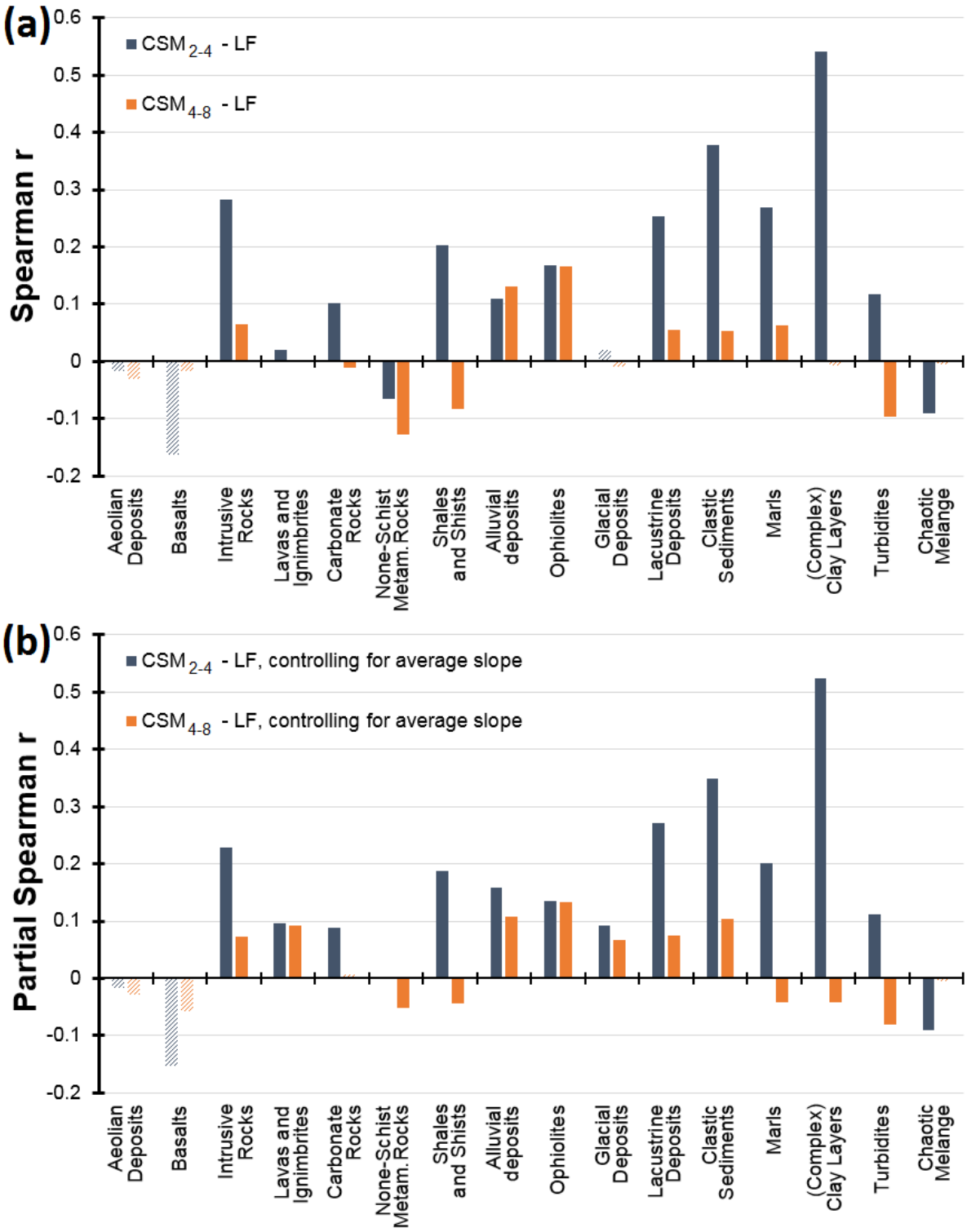

Fig. 7

Highlights

- Patterns of sediment yield and landslides across Italy are correlated to seismicity
- Correlations are much stronger for proxies relating to weak but frequent seismicity
- Seismic impacts on landslides seem to vary strongly between lithologies.
- Indirect seismic effects are likely more important than direct landslide triggering